Electrochemically Deposited Iron Sulphide Material by Adjusting the Deposition Time for Photovoltaic Application

Ernest O Ojegu[1] and Imosobomeh L Ikhioya[2]

[1] Department of Physics, Delta State University, Abraka, Delta State, Nigeria
[2] Department of Physics and Astronomy, University of Nigeria, Nsukka, 410001, Enugu State, Nigeria

Corresponding E-mail: imosobomeh.ikhioya@unn.edu.ng

Abstract

An electrochemical deposition technique was employed to synthesize FeS material. The Iron nitrate nonahydrate $(Fe(NO_3)_2.9H_2O)$ and sodium sulphate $(NaSO_4)$ are part of the electrochemical bath system. The films synthesized have a polycrystalline structure with diffraction peaks and a preferred orientation along the (111) diffraction plane. The significance of high peaks lies in their ability to provide a spacious surface area for efficient photovoltaic activities. By increasing the deposition time of FeS, the film thickness decreased from 108.98 to 100.87 nm. The FeS absorbance decreases as the wavelength approaches the VIS-IR region. The FeS material had the highest absorbance value at 30 s across the entire spectrum, averaging a maximum of 0.072 in the ultraviolet region. The films deposited had energy band gaps ranging from 2.12 to 1.58 eV. The energy band gap also decreased as the deposition time and film thickness decreased. The bandgap energy range found in this study is perfect for absorbing solar energy radiation above 1.58 eV, making it ideal for solar cell absorber layers.

Keywords: FeS; ECD; bandgap energy; photovoltaic; XRD, Resistivity.

I. INTRODUCTION

The exceptional properties of iron sulphide make it an ideal material for solar cell applications. The key components of this substance, iron and sulfur, are abundant and inexpensive to extract and process, making it non-toxic [1]–[7]. Producing these materials in large quantities can be done without high expenses. Generating clean energy and addressing global warming heavily relies on photovoltaic cells. The development of photovoltaic technology requires materials that are affordable, stable, environmentally friendly, and widely accessible [1]. Iron sulphide has caught the attention of researchers as a photovoltaic material [2]. It possesses excellent stability, is non-toxic, and has an indirect optical band gap. The most crucial aspect is its high absorption coefficient, but limited progress and use have been caused by issues such as sulfur vacancies, unwanted doping, and surface conduction. Hence, additional investigation on FeS_2 is required, including material synthesis, defect properties, and device physics [3]. Multiple techniques exist for depositing thin films of iron sulphide [1], [2], [8]–[12], [13], [14] and [15]. Electrochemical deposition offers several advantages over alternative techniques. The utilization of inexpensive equipment, low-temperature operation, and minimal waste production make this technique cost-effective and efficient [2]–[4]. Typically, researchers use a two-step process to deposit iron sulphide electrochemically. This involves direct compound electrodeposition followed by sulfurization to attain the pyrite phase.

The synthesis of single-phase iron pyrite films on ITO-

coated glass substrates was successfully carried out by Botchway et al [4]. In the experiment, a 3-electrode electrochemical system was utilized, wherein graphite acted as the counter electrode and Ag/AgCl served as the reference electrode. In a single-step process, the conductive substrate was used to directly electro-deposit the FeS precursor thin film. The deposition was carried out under room temperature conditions, utilizing a constant potential of -0.9 V vs. Ag/AgCl, in a potentiostatic manner. The iron pyrite phase was formed by annealing the as-deposited material in a sulfur-rich environment at 500°C for an hour. Two methods were used to generate sulfur gas for sulfurization: one involved Kipp's apparatus, and the other required heating elemental sulfur at 200°C. The analyzed films from both sulfurization techniques showed a pyrite phase, but the second method yielded films with improved crystalline order and stoichiometry, with no observable impurity peaks. Optical absorption measurements revealed a band gap of around 1.75 eV. The SEM micrograph showed a bumpy surface made up of unevenly shaped crystallites with clear edges, spanning the entire substrate. FeS_2 pyrite thin films were confirmed by the consistent EDAX analysis of the film.

According to Lu et al [5], iron pyrite is an affordable, stable, non-toxic, and abundant material that shows promise in photovoltaics. The low-cost method of electrochemical deposition enables researchers to prepare iron pyrite solar cells on a large scale. The synthesis of high-quality iron pyrite films was examined by electrochemically depositing them with thiourea and studying the influence of sulfurization. After the addition of sulfur, the amorphous precursor film transforms into a film of crystallized iron pyrite. Characterization reveals a band gap of 0.89 eV and classifies it as an n-type semiconductor with a carrier concentration of $3.01 \times 10^{19}\ cm^{-3}$. The light produces a response in the photovoltaic device. According to this study, sulfurization is crucial for creating pure iron pyrite films electrochemically, enabling cost-effective and large-scale production of iron pyrite solar cells.

The synthesis of FeS material involved the reduction of iron ions onto a conductive substrate through electrochemical deposition. Iron ions migrate towards the substrate and react with sulphide ions to form FeS, which is achieved by applying a voltage between the substrate and a counter electrode. Controlling parameters like applied voltage, deposition time, and electrolyte composition allow for tailored electrochemical deposition of FeS material. These parameters influence the synthesized FeS material's morphology, crystal structure, and properties. In this study, we adjusted the time for deposition. Electrochemically deposited FeS material has been utilized in different fields like energy storage, catalysis, and sensing. Its high electrochemical activity makes it a promising material for supercapacitors, batteries, and photovoltaic applications.

The study aimed to produce iron sulphide material through electrochemical deposition, to utilize it for photovoltaic by modifying the deposition time.

II. METHODS

An electrochemical deposition technique was employed to synthesize FeS material. The Iron nitrate nonahydrate $(Fe(NO_3)_2.9H_2O)$ and sodium sulphate $(NaSO_4)$ are part of the electrochemical bath system. A magnetic stirrer was used to stir the reaction bath. The power supply generated an electric field (DC voltage) by utilizing conducting glass for the cathode and carbon and fluorine electrodes for the anode. At last, we have achieved uniform thin film deposition through electrochemical deposition. The FTO-coated working electrode, measuring $2.5\ cm \times 1.5\ cm$ was fragmented and cleansed with dishwashing liquid. For the synthesis of FeS, 0.1 mol of $Fe(NO_3)_2.9H_2O$ and $NaSO_4$ were mixed. The synthesis involves the use of a three-electrode system. Platinum is used in the anode, while silver and silver chloride (Ag/AgCl) make up the reference electrode, and the cathode is constructed of FTO (fluorine-doped tin oxide). The vertical positioning of the counter and reference electrodes was within the beaker on the FTO-coated substrate. The synthesis caused maintaining a potentiostatic state of $-200\ mV$ versus SCE. The deposition time ranged from 15 to 60 s. To clean and dry the synthesized films, the hand dryer was utilized. Target materials and precursors were added in equal amounts to the beakers during the synthesis process. To ease internal stress, the films were subjected to a 20-minute annealing treatment. The optical, structural, elemental, and electrical characteristics of the synthesized materials were thoroughly assessed using appropriate tools such as X-ray diffractometer, scanning electron microscopy, and four-point probe.

III. RESULTS AND DISCUSSION

A. Structural study

The XRD result of the FeS material is depicted in Fig. 1. The films synthesized have a polycrystalline structure with diffraction peaks and a preferred orientation along the (111) diffraction plane. The significance of high peaks lies in their ability to provide a spacious surface area for efficient photovoltaic activities. The crystallinity of FeS films reduced as the peak intensity decreased with an increasing 2θ angle at a deposition time of 15 s. The low absorbance value obtained from the optical result corresponds to this outcome. The data from XRD analysis was utilized to calculate other structural parameters outlined in Table I using (1), (2), and (3) [16]–[21].

$$D = {k\lambda}/{\beta\cos\theta} \qquad (1)$$

$$d = {\lambda}/{2\sin\theta} \qquad (2)$$

$$\delta = {1}/{D^2} \qquad (3)$$

Where k = 0.94, λ = wavelength of the X-ray source given as 0.154 nm, θ = the Bragg's angle/diffraction angle. From Table I, we observed an inverse proportionality between the crystallite size and FWHM. As the FWHM angle increases, the crystallite size decreases. The deposition time was directly proportional to the size of the grains in the films, as clusters

merged to form larger grains. The improvement in FeS formation, crystallinity, and crystallite size can be attributed to this. The film's band gap changes depending on the deposition time, with a recorded band gap of 1.58 eV for a deposition time of 60 s using electrochemical deposition.

Table I. Structural values of FeS material.

| Films	2θ (degree)	d (spacing) Å	(Å)	(β)	(hkl)	(D) nm	$\sigma lines/m^2 \times 10^{16}$
FeS, 15 s	13.308	6.652	11.521	0.956	111	0.146	1.426
	17.382	5.101	10.202	0.958	200	0.146	1.418
	19.565	4.536	9.073	0.959	211	0.146	1.412
	22.585	3.936	8.801	0.961	311	0.147	1.405
FeS, 30 s	13.999	6.325	10.955	0.889	111	0.157	1.233
	17.876	4.961	9.922	0.886	200	0.158	1.213
	19.765	4.491	8.982	0.885	211	0.159	1.203
	22.962	3.872	8.659	0.881	311	0.160	1.180
FeS, 40 s	13.999	6.325	10.955	0.883	111	0.158	1.216
	17.876	4.961	9.922	0.886	200	0.158	1.213
	19.765	4.491	8.982	0.889	211	0.158	1.214
	22.962	3.872	8.659	0.892	311	0.158	1.210
FeS, 60 s	13.999	6.325	10.955	0.894	111	0.156	1.247
	17.876	4.961	9.922	0.997	200	0.140	1.536
	19.765	4.491	8.982	0.898	211	0.156	1.238
	22.962	3.872	8.659	0.899	311	0.157	1.229
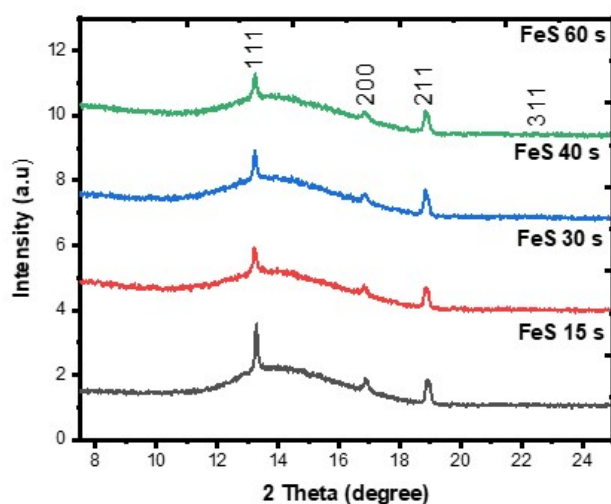
Fig. 1 XRD pattern of FeS material.

B. Resistivity and conductivity of FeS material

Table II displays the electrical analysis of FeS materials. By increasing the deposition time of FeS, the film thickness decreased from 108.98 to 100.87 nm. Fig. 2 shows the relationship between resistivity and conductivity in a semiconductor material as the film thickness decreases.

Table II. Electrical properties of FeS nanostructured material.

Samples	Thickness, t (nm)	Resistivity, ρ $(\Omega m) \times 10^{-6}$	Conductivity, σ $(S/m) \times 10^{-8}$
FeS, 15 s	108.98	89.49	1.11
FeS, 30 s	103.76	86.72	1.15
FeS, 40 s	102.56	85.89	1.16
FeS, 60 s	100..87	79.59	1.25

The enhanced conductivity of created materials allows for the advancement of potential solar device materials. The deposition time of FeS_2 material has a significant impact on its resistivity and conductivity. Increasing deposition times leads to decreased resistivity and increased conductivity. The duration of deposition impacts the structural characteristics of FeS_2 material. Increased deposition times enhance the growth of bigger and more crystalline grains, resulting in enhanced electrical conductivity [22]–[24]. To optimize the performance of iron sulphide material in applications like solar cells, batteries, and sensors, it is important to understand how deposition time affects its electrical properties.
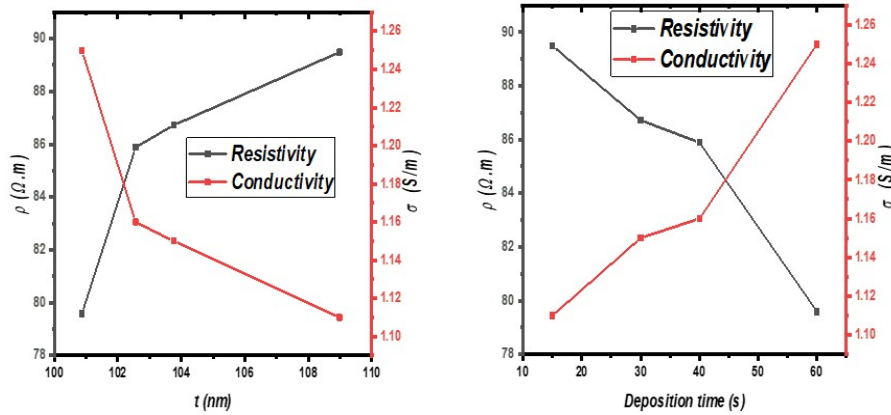
Fig. 2 Resistivity and conductivity of FeS material.

C. Optical study

Equations (4) and (5) afford the relationship between Absorbance, Transmittance and Reflectance of a material.

$$T = 10^{-A} \tag{4}$$

$$R = 1 - (A + T) \tag{5}$$

Where A = Absorbance, T = Transmittance, and R = Reflectance [16]–[21].

The absorbance of FeS materials is shown in Fig. 3. The FeS absorbance decreases as the wavelength approaches the VIS-IR region. The FeS material had the highest absorbance value at 30 s across the entire spectrum, averaging a maximum of 0.072 in the ultraviolet region. The absorbance spectra decreased due to deposition time. The reason for this could be attributed to the observed rise in the crystallite peak in the XRD pattern, subsequently leading to an increase in the size of FeS. The high absorbance displayed by these films in the near-infrared and visible spectrum makes them ideal for forming p-n junctions in solar cells and other photovoltaic applications. The absorption of iron sulphide material depends heavily on the duration of deposition. Increased deposition times lead to higher absorbance as the film becomes thicker and more crystalline. Achieving desired absorbance properties heavily relies on determining the optimal deposition time. The relationship between deposition time and absorbance is commonly studied by researchers through experiments, to find the ideal time for achieving the highest absorbance in a specific application. Controlled absorbance properties of iron sulphide materials are utilized in multiple fields such as solar cells, photodetectors, and electrochemical devices. Tailoring these materials for specific applications requires understanding the impact of deposition time on absorbance [25]. The transmittance values were determined from the absorbance values using (4) and Fig. 4. The results show that FeS has higher transmittance in the VIS-IR spectrum, showing its potential for photovoltaic devices. The films showed high

transmittance (> 90%) in the UV region. The films that were deposited at 30 s had the highest transmittance, averaging 93% in the visible and near-infrared range. The transmittance of iron sulphide material is greatly influenced by the deposition time. The transmittance increases as the deposition time lengthens, thanks to the formation of larger and more crystalline grains. The transmittance of the iron sulphide material is also affected by its crystallinity and defect density. Higher transmittance is achieved through higher crystallinity and fewer defects. The transmittance of the iron sulphide material is also impacted by its band gap. Higher transmittance in the visible spectrum is a result of a wider band gap. Fig. 5 shows that all the films deposited had very low reflectance values, as evaluated using (5). The reflectance values slightly increased from ultraviolet to visible, remaining relatively constant in the visible and near-infrared regions. The reflectance value of every film that was deposited was over 15%. Window layers in photovoltaic applications benefit from their low reflectance, especially in the Visible region. The reflectance of iron sulphide material is affected by the deposition time. Increased deposition times result in greater reflectance values. The deposited film's increased thickness and improved crystallinity are responsible for this. The optical properties of iron sulphide material are also influenced by the deposition time. Films with longer deposition times exhibit reduced bandgap energies and increased absorption coefficients. As the deposition time increases, the material becomes more conductive and absorbs more light. The fabrication of iron sulphide materials heavily relies on the crucial parameter of deposition time. By optimizing the deposition time, researchers can customize the optical and electrical properties of the material for specific applications. Fig. 6 depicts the correlation between $(\alpha h v)2$ and $h v$ in FeS material. The energy band gaps of the material were determined by extrapolating the graph's linear region to $(\alpha h v)2 = 0$. The films deposited had energy band gaps ranging from 2.12 to 1.58 eV. As the deposition time and film thickness decreased, the energy band gap also decreased. The

bandgap energy range found in this study is perfect for absorbing solar energy radiation above 1.58 eV, making it ideal for solar cell absorber layers. Increasing the deposition time has been found to cause a decrease in the band-gap energy of iron sulphide material. The band-gap energy of iron sulphide material can vary depending on the deposition period. Iron sulphide's properties, including crystallinity and iron content, are influenced by the deposition period.
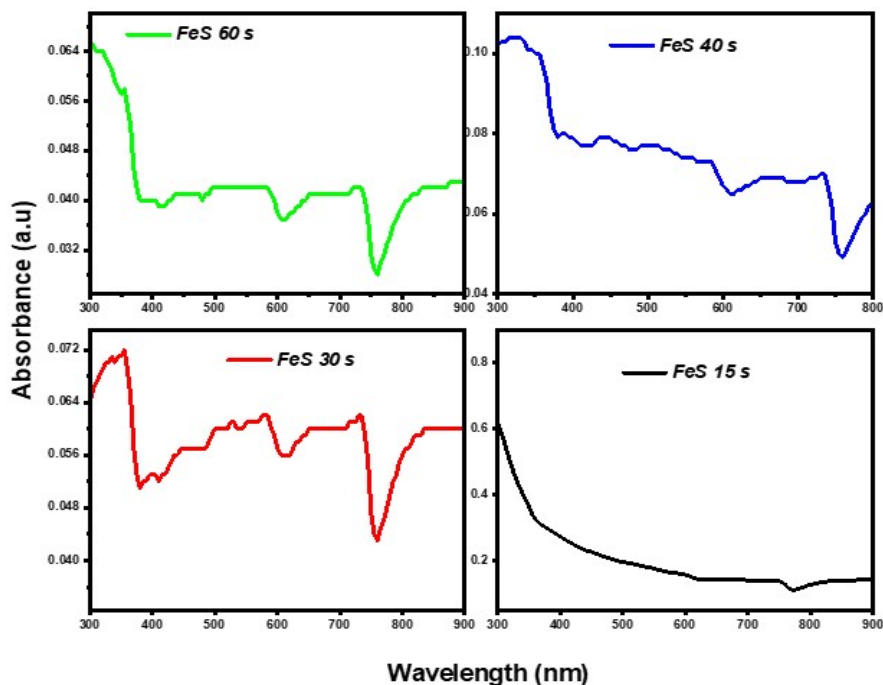
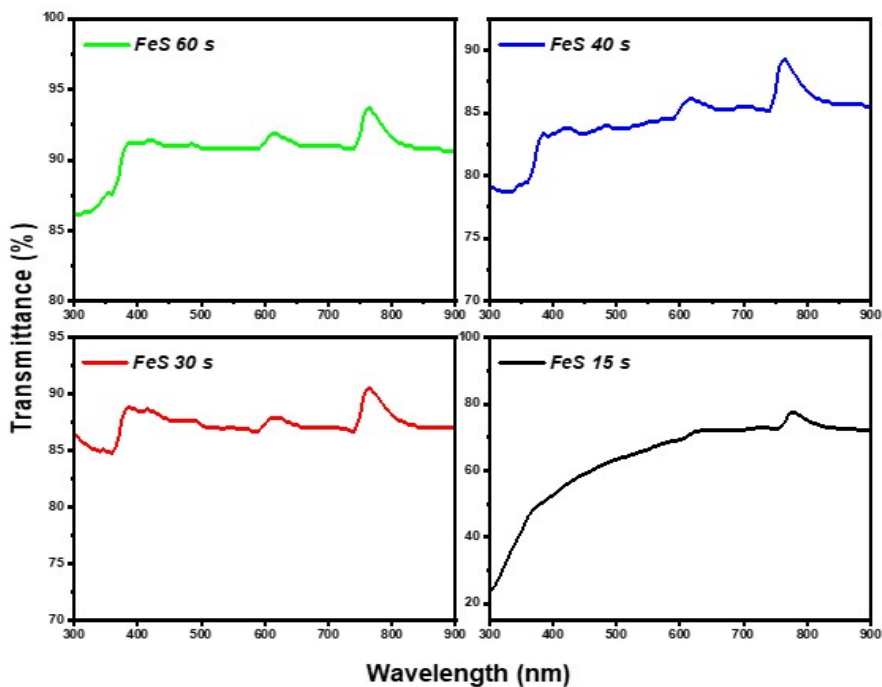

Fig. 3 absorbance of FeS material.
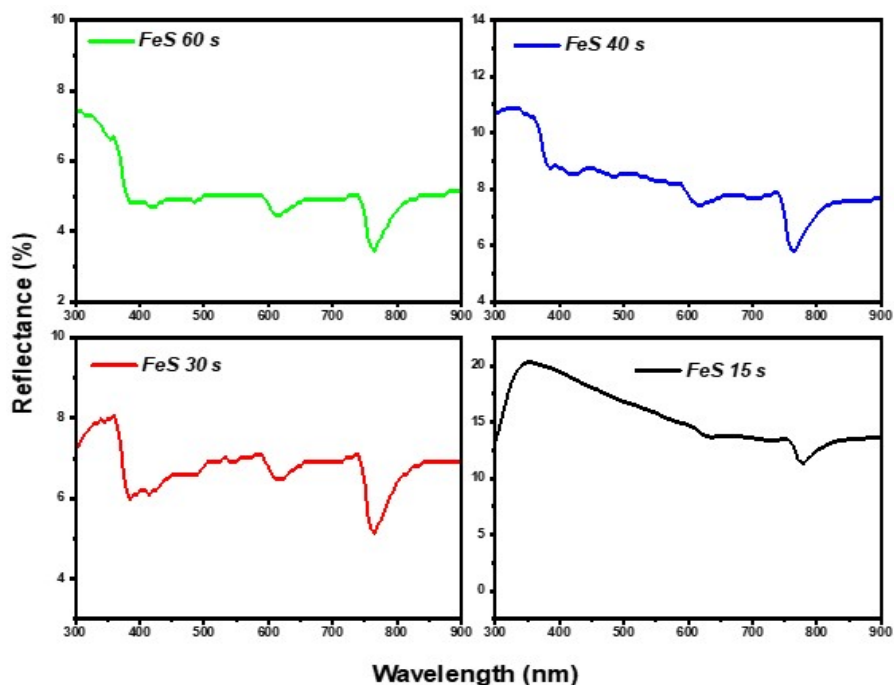

Fig. 4 Transmittance of FeS material.
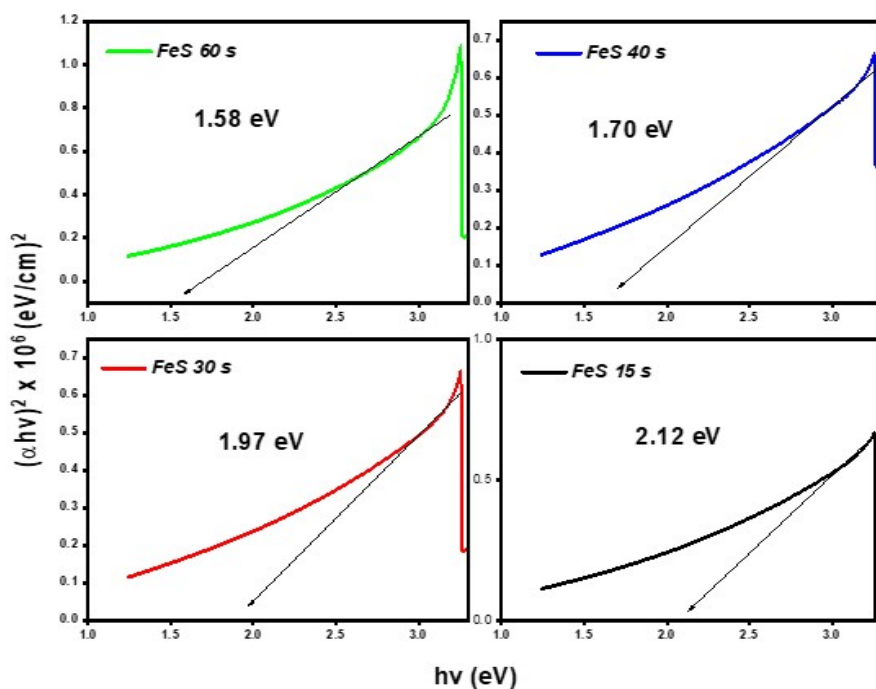
Fig. 5 reflectance of FeS material.

Fig. 6 Bandgap energy of FeS material.

The energy bandgap of FeS nanostructured materials is significantly affected by the deposition time. The longer the deposition time, the smaller the bandgap becomes. Longer deposition times result in changes to the film's morphology, increased thickness, and improved crystallinity. The

sulfurization temperature also influenced the bandgap of FeS nanostructured materials [17], [23], [24], [26]–[32], [33]–[40]. A lower bandgap is observed at higher temperatures. The choice of sulfurization agent can impact the bandgap. The decrease in bandgap is likely a result of multiple factors

associated with increasing deposition time. A potential outcome is the creation of a greater quantity of defect states in the bandgap, serving as intermediate points for electron transitions. A thinner material can enhance the interaction between electrons and lattice vibrations, resulting in a narrower bandgap. The ability to adjust the energy bandgap by altering deposition time presents exciting opportunities to customize FeS nanomaterials for specific uses. Solar energy conversion benefits from materials with a smaller bandgap, while electronic devices favour those with a larger bandgap.

IV. CONCLUSION

FeS material has been synthesized successfully using the Electrochemical deposition technique. The synthesized films exhibit a polycrystalline structure, with diffraction peaks and a preferred orientation along the (111) diffraction plane. High peaks are important because they offer a large surface area for effective photovoltaic activities. The film thickness decreased from 108.98 to 100.87 nm by increasing the deposition time of FeS. The absorbance of FeS decreases as the wavelength gets closer to the VIS-IR region. At 30 s, the FeS material showed the highest absorbance value throughout the spectrum, with an average maximum of 0.072 in the ultraviolet region. The films exhibited UV transmittance above 90%. Films deposited at 30 s exhibited the highest transmittance, with an average of 93% in the visible and near-infrared range. The deposition time has a significant impact on the transmittance of iron sulphide material. The deposited films exhibited energy band gaps between 2.12 and 1.58 eV. Decreasing the deposition time and film thickness led to a decrease in the energy band gap. The study discovered a bandgap energy range ideal for absorbing solar radiation above 1.58 eV, making it perfect for solar cell absorber layers.

CREDIT AUTHOR STATEMENT

Ernest O Ojegu and Imosobomeh L. Ikhioya: conceptualization, methodology, Data curation, Imosobomeh L. Ikhioya: data collection, first-draft writing, reviewing, software, and editing. Investigation and visualization. All authors approved the submission.

CONFLICT OF INTEREST

The authors confirm that there are no personal or financial conflicts that may have influenced the study's findings.

AVAILABILITY OF DATA

Data is made freely available on request.

ACKNOWLEDGEMENT

References

[1] J. Puthussery, S. Seefeld, N. Berry, M. Gibbs, and M. Law, "Colloidal iron pyrite (FeS_2) nanocrystal inks for thin-film photovoltaics," J. Am. Chem. Soc., vol. 133, no. 4, pp. 716–719, 2011, doi: 10.1021/ja1096368.

[2] R. Schieck, A. Hartmann, S. Fiechter, R. Könenkamo, and H. Wetzel, "Electrical Properties of Natural and Synthetic Pyrite (FeS_2) Crystals," J. Mater. Res., vol. 5, no. 7, pp. 1567–1572, 1990, doi: 10.1557/JMR.1990.1567.

[3] D. Spagnoli, K. Refson, K. Wright, and J. D. Gale, "Density functional theory study of the relative stability of the iron disulphide polymorphs pyrite and marcasite," Phys. Rev. B - Condens. Matter Mater. Phys., vol. 81, no. 9, 2010, doi: 10.1103/PhysRevB.81.094106.

[4] E. A. Botchway, F. K. Ampong, I. Nkrumah, F. K. Boakye, and R. K. Nkum, "Growth of a Pure and Single-Phase Iron Sulphide (Pyrite) Thin Film by Electrochemical Deposition for Photovoltaic Applications," Open J. Appl. Sci., vol. 09, no. 09, pp. 725–735, 2019, doi: 10.4236/ojapps.2019.99059

[5] Z. Lu, H. Zhou, C. Ye, S. Chen, J. Ning, M. A. Halim, S. B. Donaev and S. Wang, "Fabrication of Iron Pyrite Thin Films and Photovoltaic Devices by Sulfurization in Electrodeposition Method". Nanomat., vol. 11, 2021. https://doi.org/10.3390/nano11112844.

[6] A. Walimbe et al., "Influence of substrate temperature on properties of pyrite thin films deposited using a sequential coevaporation technique," Thin Solid Films, vol. 669, pp. 49–55, 2019, doi: 10.1016/j.tsf.2018.10.022.

[7] X. Wang et al., "Pyrite thin films prepared for thermal batteries via sulfuring electrodeposited iron sulphide films: Structure and physical properties," Mat. Lett., vol. 110, pp. 144–147, 2013, doi: 10.1016/j.matlet.2013.07.107.

[8] E. A. Botchway, F. K. Ampong, I. Nkrumah, F. K. Boakye, and R. K. Nkum, "Growth of a Pure and Single-Phase Iron Sulphide (Pyrite) Thin Film by Electrochemical Deposition for Photovoltaic Applications," Open J. Appl. Sci., vol. 09, no. 09, pp. 725–735, 2019, doi: 10.4236/ojapps.2019.99059.

[9] M. Cabán-Acevedo, M. S. Faber, Y. Tan, R. J. Hamers, and S. Jin, "Synthesis and properties of semiconducting iron pyrite (FeS_2) nanowires," Nano Lett., vol. 12, no. 4, pp. 1977–1982, 2012, doi: 10.1021/nl2045364.

[10] C. T. Kao et al., "Temperature-Dependent Effects of FeS_2 Thin Film Synthesized by Thermochemical Spraying: An Optical and Physicochemical Investigation," J. Therm. Spray Tech., vol. 25, no. 3, pp. 580–586, 2016, doi: 10.1007/s11666-016-0379-7.

[11] G. Kaur, M. Kaur, A. Thakur, and A. Kumar, "Recent Progress on Pyrite FeS_2 Nanomaterials for

Energy and Environment Applications: Synthesis, Properties and Future Prospects," J. Clust. Sci., vol. 31, no. 5, pp. 899–937, 2020, doi: 10.1007/s10876-019-01708-3.

[12] S. Kawai, R. Yamazaki, S. Sobue, E. Okuno, and M. Ichimura, "Electrochemical deposition of iron sulphide thin films and heterojunction diodes with zinc oxide," APL Mater., vol. 2, no. 3, 2014, doi: 10.1063/1.4869035.

[13] S. Khalid, E. Ahmed, Y. Khan, K. N. Riaz, and M. A. Malik, "Nanocrystalline Pyrite for Photovoltaic Applications," ChemistrySelect, vol. 3, no. 23, pp. 6488–6524, 2018, doi: 10.1002/slct.201800405.

[14] S. Kment et al., "Epoxy catalyzed sol-gel method for pinhole-free pyrite FeS2 thin films," J. Alloys Compd., vol. 607, pp. 169–176, 2014, doi: 10.1016/j.jallcom.2014.04.060.

[15] Z. Lu et al., "Fabrication of iron pyrite thin films and photovoltaic devices by sulfurization in electrodeposition method," Nanomat., vol. 11, no. 11, 2021, doi: 10.3390/nano11112844.

[16] N. I. Akpu, C. A. Sylvanus, and E. C. Nwaokorongwu, "Modulation of the physical properties of spray-deposited cobalt selenide nanofilm via yttrium doping for photovoltaic purposes," J. Mater. Env. Sci., vol. 14, no. 11, pp. 1230–1244, 2023.

[17] N. Akpu et al., "Impact of temperature difference on the features of spray deposited yttrium doped cobalt selenide (YCoSe) thin films for photovoltaic application," Afr. Sci. Reports, vol. 2, p. 143, 2023, doi: 10.46481/asr.2023.2.3.143.

[18] A. Ali, S. Afzal, T. Khaleeq, H. Shah, M. Usman, and L. Imosobomeh, "Synthesis and Characterization of Chitosan-Silver Nanocomposite Using Chemical Reduction Method and their Antibacterial Properties," J. of Nano & Mater. Sci. Res. (JNMSR) vol. 2, no. 1, pp. 117–122, 2023.

[19] I. L. Ikhioya and A. C. Nkele, "A Novel Synthesis of Hydrothermally Prepared Europium Sulphide and Cerium Sulphide Nanomaterials Doped with Yttrium," Arab. J. Sci. Eng., 2023, doi: 10.1007/s13369-023-08292-9.

[20] I. L. Ikhioya and A. C. Nkele, "Properties of electrochemically deposited NiTe films prepared at varying dopant concentrations of molybdenum," J. Mat. Sci. Mat. Elect., vol. 34, no. 21, 2023, doi: 10.1007/s10854-023-11018-0.

[21] I. L. Ikhioya, A. C. Nkele, and F. U. Ochai-Ejeh, "Green synthesis of copper oxide nanoparticles using neem leaf extract (Azadirachta indica) for energy storage applications," Mat. Res. Innov., pp. 1–7, 2023.
doi: 10.1080/14328917.2023.2252677.

[22] I. L. Ikhioya et al., "Electrochemical engineering of ZIF-7 electrode using ion beam technology for better supercapacitor performance," J. Energy Storage, vol. 90, no. PA, pp. 111833, 2024, doi: 10.1016/j.est.2024.111833.

[23] I. L. Ikhioya and A. C. Nkele, "Green synthesis and characterization of aluminium oxide nanoparticle using neem leaf extract (Azadirachta Indica)," Hybrid Adv., vol. 5, no. November 2023, pp. 100141, 2024, doi: 10.1016/j.hybadv.2024.100141.

[24] C. Uchechukwu, A. Osita, J. Chukwuemeka, I. Lucky, and O. Odira, "Investigating the influence of natural dye extracts from Ocimum gratissimum, Solanum melongena, Piper guineese, and their blend in the fabrication of perovskite solar cells," Hybrid Adv., vol. 6, no. April, p. 100198, 2024, doi: 10.1016/j.hybadv.2024.100198.

[25] O. O. Ernest and O. O. E. Enaroseha, "Optical properties of the anatase phase of titanium dioxide thin films prepared by electrostatic spray deposition," Nig. J. of Sci. & Env., vol. 18, no. 2, 2020.
https://delsunjse.com/index.php/njse/article/view/33

[26] H. Shah, S. Afzal, M. Usman, K. Shahzad, and I. L. Ikhioya, "Impact of Annealing Temperature on Lanthanum Erbium Telluride (La0.1Er0.2Te0.2) Nanoparticles Synthesized via Hydrothermal Approach," Adv. J. Chem. Sect. A, vol. 6, no. 4, pp. 342–351, 2023, doi: 10.22034/AJCA.2023.407424.1386.

[27] K. I. Udofia, I. L. Ikhioya, D. N. Okoli, and A. J. Ekpunobi, "Impact of doping on the physical properties of PbSe chalcogenide material for photovoltaic application," Asian J. Nanosci. Mater., vol. 6, no. 2, pp. 135–147, 2023, doi: 10.26655/AJNANOMAT.2023.2.3.

[28] I. Rufus and I. L. Ikhioya, "Enhanced Electrical, Morphology, Structural, and Optical Features of Nickel Silver Sulphide Material," J. of Basic Phy. Res., vol. 11, no. 2, pp. 1–9, 2023.

[29] S. O. Samuel, M. L. E. Frank, E. P. Ogherohwo, A. Ekpekpo, J. T. Zhimwang, and I. L. Ikhioya, "Influence of Deposition Voltage on Strontium Sulphide Doped Silver for Optoelectronic Application," East Eur. J. Phys., vol. 2023, no. 1, pp. 189–196, 2023, doi: 10.26565/2312-4334-2023-1-25.

[30] P. Kumar, V. Sharma, A. Kumar, K. Sachdev, and K. Asokan, " Structural, morphological and vibrational properties of Fe2O3 nanoparticles," Macromolecular Symposia, 400 (1), 2100033.vol. 2, no. 1, pp. 163–163, 2016, doi: 10.3850/978-981-09-7519-7nbl16-rps-163.

[31] L. A. Nnannaa, U. Joseph, E. C. Nwaokorongwu, U. A. Ezere, N. I. Akpu, and I. L. Ikhioya, "Impact of annealing temperature on praseodymium cerium telluride nanoparticles synthesise via hydrothermal approach for optoelectronic application," Mater. Res. Innov., vol. 00, no. 00, pp. 1–11, 2024, doi: 10.1080/14328917.2024.2320982.

[32] S. O. Malumi, T. Malumi, M. O. Osiele, and I. L. Ikhioya, "Enhance and Performance Evolution of Silver-Doped Titanium Dioxide Dye-Sensitized Solar Cells Using Different Dyes," J. of Eng. in Ind. Res., vol. 4, no. 4, pp. 189–200, 2023. https://doi.org/10.48309/jeires.2023.4.1

[33] E. O. Ojegu, S. O. Samuel, M. O. Osiele, G. E. Akpojotor, and I. L. Ikhioya, "Optimisation of deposition voltage of zirconium-doped chromium telluride via typical three-electrode cell electrochemical deposition technique," Mat. Res. Innov., vol. 00, no. 00, pp. 1–9, 2023, doi: 10.1080/14328917.2023.2243063.

[34] I. Okeoghene Blessing, H. Shah, S. Afzal, and I. L. Ikhioya, "Enhanced structural properties of electrochemically synthesised NiFeS using 500 keV carbon C++ ions irradiation," Mat. Res. Innov., 2023, doi: 10.1080/14328917.2023.2262315.

[35] A. Hussain, S. Habib, I. Ullah, F. Sahreen, I. Ahmad, I. L. Ikhioya, Enhanced Structural, Morphological and Optical Features of Tix MnNiO (X= 1, 2, and 3 mL) Synthesized Using Hydrothermal Approach. Eurasian J. Sci. Tech., vol. 4, no. 3, pp. 195-207, 2024.
https://doi.org/10.48309/EJST.2024.428429.1117

[36] A. Hussain, F. Ali, and H. Hammad, "Enhanced specific capacitance, structural, optical, and morphological study of carbon ions incorporated into the lattice of $ZrCuO_2$ nanoparticle synthesized by hydrothermal method," Hybrid Adv., vol. 5, no. January, pp. 100170, 2024.
doi: 10.1016/j.hybadv.2024.100170.

[37] A. U. Rehman, T. Munir, S. Afzal, M. Saleem, I. L. Ikhioya, "Enhanced Solar Cell Efficiency with Tin-Based Lead-Free Material ($FASnI_3$) through SCAPS-1D Modeling". Eurasian J. Sci. Tech., vol. 4, no. 3, pp. 244-252, 2024.

[38] S. G. Sarwar, I. L. Ikhioya, S. Afzal, and I. Ahmad, "Supercapitance performance evaluation of MXene / Graphene / NiO composite electrode via in situ precipitation technique," Hybrid Adv., vol. 4, no. September, pp. 100105, 2023, doi: 10.1016/j.hybadv.2023.100105.

[39] I. Rufus, A. Peter, S. O. Aisida, and I. L. Ikhioya, "Results in Optics Influence of manganese molarity incorporation on manganese silver sulphide semiconductor material for photovoltaic applications," Results Opt., vol. 12, no. February, pp. 100464, 2023, doi: 10.1016/j.rio.2023.100464.

[40] B. C. N. Obitte et al., "The effects of doping and temperature on properties of electrochemically deposited Er3+ doped ZnSe thin films," Opt. Mater. (Amst)., vol. 124, no. December 2021, pp. 111979, 2022, doi: 10.1016/j.optmat.2022.111979.